Applied Catalysis B: Environment and Energy 347 (2024) 123788

Contents lists available at ScienceDirect

Applied Catalysis B: Environment and Energy

journal homepage: www.elsevier.com/locate/apcatb

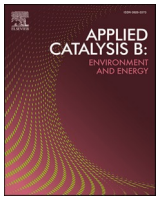

Alkali-resistant catalytic reduction of NO_x over CeO_2-WO_3/MCM-22 supported catalyst by releasing Brønsted acid sites

Lei Chen [a], Yu Zou [a], Yonglong Li [a], Guobo Li [a,*], Wenming Liu [b], Hongxiang Zhang [a], Shengyong Lu [c], Zhenguo Li [d], Shule Zhang [e], Honggen Peng [a,b,**]

[a] School of Resources and Environment, Nanchang University, 999 Xuefu Road, Nanchang, Jiangxi 330031, PR China
[b] School of Chemistry and Chemical Engineering, Nanchang University, 999 Xuefu Road, Nanchang, Jiangxi 330031, PR China
[c] State Key Laboratory for Clean Energy Utilization, Institute for Thermal Power Engineering, Zhejiang University, Hangzhou 310027, PR China
[d] National Engineering Laboratory for Mobile Source Emission Control Technology, China Automotive Technology & Research Center, Tianjin 300300, PR China
[e] School of Chemical Engineering, Nanjing University of Science and Technology, Nanjing 210094, PR China

ARTICLE INFO

Keywords:
Air pollution control
NO_x removal
Molecular sieve catalyst
Anti–K poisoning
Mechanism

ABSTRACT

The CeO_2–WO_3 catalyst used for NO_x abatement in biomass boiler combustion was prone to severe deactivation due to the high alkali metal content in exhaust gas. Enhancing the alkali resistance of the CeO_2–WO_3 catalyst was crucial for its practical application. In this study, the CeO_2–WO_3/MCM-22 catalysts were synthesized via a simple impregnation method, resulting in a minimal reduction in catalyst activity after 1 wt% K_2O poisoning. The anti-K poisoning mechanism of CeO_2–WO_3/MCM-22 catalyst was studied. The results demonstrated that the acid sites of lamellar MWW-Type molecular sieve MCM-22 (Mobil composition of matter-22) acted as sacrificial sites, effectively trapping the alkali poisoning and protecting the CeO_2–WO_3 active component. Compared with CeO_2–WO_3 catalyst, the Brønsted acid sites on the cerium tungstate occupied by foreign K, were liberated as K element preferentially bound to the molecular sieve MCM-22.

1. Introduction

The emission of nitrogen oxides (NO_x) from human production and transportation processes gives rise to detrimental environmental impacts, including acid rain, photochemical smog, and haze that degrades the ecological environment [1–3]. Importantly, NH_3-SCR technology can convert NO_x into N_2 and H_2O, the core of technology is development of efficient catalyst [4]. The commercial V_2O_5–WO_3/TiO_2 catalyst possesses satisfactory NO_x removal performance and splendid resistance to water (H_2O) and Sulphur dioxide (SO_2) at medium and high temperatures (300–400 ℃). However, the vanadium species of V_2O_5–WO_3/TiO_2 catalyst are toxic and the catalyst is prone to cumulative deactivation due to alkali metals (K, Na) presented in exhaust gas. Commercial catalysts applied in power plants and industrial boilers require replacement or regeneration operations every 2–5 years, which significantly increases operational costs [5–7]. Additionally, owing to the promotion of sustainable development concepts and the improvement of environmental quality requirements, biomass fuels will substitute conventional fossil fuels, leading to an increase in alkali metal content in exhaust gas and expedited deactivation of catalysts [8,9]. Hence, there is a pressing need to design an environmentally friendly and robust *de*NO_x catalyst with remarkable alkali metal tolerance.

Currently, researchers have designed catalysts with high alkali tolerance by doping with elements (metal or nonmetal), separating catalytic active sites and toxic capture sites, and using appropriate carriers. Zhang et al. [10] investigated the B-doped CeO_2/TiO_2 catalyst. The results indicated that the Ce–O–B sites formed by B doping could preferentially bind with K, which effectively alleviates catalyst poisoning by K. Feng et al. [9] prepared $Fe_2(SO_4)_3$/TiO_2 catalyst with remarkable tolerance to alkali metals, which was attributable to the interaction between the active sites and poisoning sites. Ji et al. [11] synthesized a CeMn–ZSM-5 hybrid catalyst, which expressed ~10% reduction in activity after 2 wt% K_2O poisoning. The results revealed that this was primarily due to the preferential combination of K poisons with the Lewis (L) acid sites of molecular sieve ZSM-5. Chen et al. [12] synthesized sulfated CeO_2 catalysts through a simple impregnation method. The surface $Ce_2(SO_4)_3$ species can preferentially combine with K, while the active sites were reserved, endowing the sulfated CeO_2

* Corresponding author.
** Corresponding author at: School of Resources and Environment, Nanchang University, 999 Xuefu Road, Nanchang, Jiangxi 330031, PR China.
E-mail addresses: liguobo@ncu.edu.cn (G. Li), penghonggen@ncu.edu.cn (H. Peng).

https://doi.org/10.1016/j.apcatb.2024.123788
Received 12 December 2023; Received in revised form 25 January 2024; Accepted 28 January 2024
Available online 1 February 2024

catalyst with prominent tolerance to K. Zhou et al. [13] employed TiO_2 pillared montmorillonite with self-created targeted anti-poisoning sites as support, which effectively prevented active CeO_2 component from being poisoned. In summary, introducing sacrificial sites to anchor alkali poisons is a feasible method to enhance the alkali resistance of the catalyst, thereby preserving the active sites.

CeO_2 possesses a unique versatile structural arrangement and electronic features, which endow it with excellent redox properties and remarkable oxygen storage capacity (OSC), making it potentially efficient substitute for vanadium–based catalysts [14,15]. Nonetheless, due to the insufficient acidity of single CeO_2 catalyst, its catalytic performance is not satisfactory. Therefore, a second additive is usually added to enhance the catalytic performance of the CeO_2 catalyst. Shan et al. [16] prepared a new CeO_2–WO_3 catalyst with outstanding activity at medium and high temperatures. It was observed that tungsten oxide provided acidity and there was a synergistic effect between cerium and tungsten species. Peng et al. [17] investigated that alkali metals deactivate CeO_2–WO_3 catalyst. The results showed that the catalyst deactivation was attributable to the reduction of reducibility and the quantity of B acid sites. Subsequently, Peng et al. [18] studied the active site of CeO_2–WO_3 catalyst and both acid and redox cycle exist on the CeO_2–WO_3 catalyst. However, severe deactivation of the CeO_2–WO_3 catalyst due to the alkali metals (K, Na) presented in the exhaust emissions is currently a major challenge for practical applications. Mobil composition of matter-22 (MCM-22) is a layered MWW-Type molecular sieve with two sets of independent pore structures. One is a two-dimensional sinusoidal channel with an elliptical ring cross section (4.1 ×5.1 Å), and the other is a cylindrical 12-member-ring super-cage (7.1 ×7.1 ×18.2 Å) [19,20]. MCM-22 possesses characteristics of a large specific surface area (usually 400–500 $m^2 \cdot g^{-1}$), excellent thermal/hydrothermal stability, strong adsorption capacity and tunable acidity over a wide range. These properties endow MCM-22 with a significant ability to anchor foreign alkali poisons and protect the active component.

In this study, diverse CeO_2–WO_3/MCM-22 catalysts were synthesized using a simple impregnation method. The catalysts exhibited minimal reduction in activity after 1 wt% K_2O poisoning and maintained good activity after 2 wt% K_2O poisoning. The properties and reaction mechanism of the CeO_2–WO_3 and CeO_2–WO_3/MCM-22 catalysts were systematically studied through experiments and DFT calculations. Characterization results showed that the acid sites of lamellar MWW-type molecular sieve MCM-22 acted as sacrificial sites to trap K poisons, protecting the active CeO_2–WO_3 component. Meanwhile, the DFT calculations further confirmed that K was trapped in the molecular sieve MCM-22, which corresponded to experimental results. Moreover, through recombination with MCM-22, the B acid sites on the Ce-W occupied by K were liberated. This enabled the maintenance of high-efficiency acid site cycling (NH_3 adsorption) and the restoration of the catalytic reaction path. The research conducted in this study establishes a theoretical foundation for the development of an environmentally friendly and robust *de*NO_x NH_3-SCR catalyst with exceptional resistance to K.

2. Materials and methods

2.1. Catalyst synthesis

The x%CeO_2–WO_3/MCM-22 (x = 10, 20, and 30) catalysts were synthesized via the impregnation method. For comparison, the CeO_2–WO_3 was synthesized via the co-precipitation method. K-poisoned CeO_2–WO_3/MCM-22-y%K or CeO_2–WO_3-y%K (y = 1, 1.5, and 2) catalysts were simulated via the impregnation method. The detailed preparation process for these catalysts is shown in Supplementary material (SM).

2.2. Catalytic performance evaluations

The *de*NO_x performance of the obtained catalysts was evaluated in a self-assembled fixed-bed quartz reactor with continuous flow. The testing details of catalytic activity, kinetics experiments, catalyst characterization and DFT calculation are shown in the SM.

3. Results and discussion

3.1. DeNO_x performance and K resistance analysis

According to the Fig. S1, the 20%CeO_2–WO_3/MCM-22 (CeO_2–WO_3/MCM-22 for short) exhibited the optimal catalytic activity and was selected for all subsequent analyses. Fig. 1 illustrates the NO_x conversion, N_2 selectivity and N_2O concentration of CeO_2–WO_3, CeO_2–WO_3/MCM-22, CeO_2–WO_3-y%K and CeO_2–WO_3/MCM-22-y%K catalysts across the temperature range of 100–600 ℃. CeO_2–WO_3-1%K catalyst significantly loss of activity with maximum 40% NO_x conversion at 325 ℃. For comparison, CeO_2–WO_3/MCM-22–1%K catalyst reached 100% NO_x conversation at 325 ℃ and maintained good catalytic activity within the temperature range of 275–550 ℃ (Fig. 1a). Meanwhile, The CeO_2–WO_3 and CeO_2–WO_3/MCM-22 catalyst exhibited high N_2 selectivity (> 90%) and low N_2O concentration (< 10 ppm) between 200–600 ℃ (Fig. 1b). Moreover, with an increase of K loading from 1–2 wt%, no noticeable decrease in activity was observed on CeO_2–WO_3/MCM-22 and the catalytic activity reached over 95% NO_x conversion at 300 ℃, showcasing the remarkable K resistance of the catalyst (Fig. 1c). In contrast, CeO_2–WO_3 catalyst exhibited low K resistance, with almost complete deactivation observed when the K_2O loading reached 2 wt% (Fig. 1d). In addition, the intrinsic activation energy (E_a) of the CeO_2–WO_3/MCM-22 and CeO_2–WO_3/MCM-22–1%K catalysts were also evaluated. The NO_x conversion remained below < 15% to eliminate the effects of internal and external diffusion (Fig. S3). The E_a of the fresh CeO_2–WO_3/MCM-22 catalyst was 78 $kJ \cdot mol^{-1}$. After K poisoning, the E_a of CeO_2–WO_3/MCM-22–1%K catalyst slightly increased to 80 $kJ \cdot mol^{-1}$, which was consistent with the activity tests of CeO_2–WO_3/MCM-22 and CeO_2–WO_3/MCM-22–1%K. To explore the reason for the high resistance of catalyst to K poisoning, CeO_2–WO_3/MCM-22–1%K (CeO_2–WO_3/MCM-22–1%K for short) with exceptional resistance to K was selected for all subsequent analyses.

3.2. Chemical states analysis

Raman spectroscopy analysis was performed on CeO_2–WO_3, CeO_2–WO_3/MCM-22, CeO_2–WO_3-K and CeO_2–WO_3/MCM-22-K, to further characterize the presence of components on the surface of the catalyst (Fig. S9). A peak at 464 cm^{-1}, corresponding to the $F_{2\,g}$ pattern of the symmetrical vibration of oxygen atoms around the Ce in CeO_2 of cubic fluorite was observed. Additionally, a peak at 969 cm^{-1}, attributable to the stretching vibration pattern of heteropolymorphism species $WO_{2(t)}$ was observed [18,21,22]. The peak intensity of CeO_2–WO_3-K and CeO_2–WO_3/MCM-22-K at 460 cm^{-1} was increased, indicating Ce aggregation caused by K. The Raman spectroscopy result was consistent with the XRD analysis.

The reducibility property of a catalyst is significant for its deactivation, with Alkali metals like K usually reducing this property [23–25]. Therefore, it was important to investigate changes in the reducibility performance over CeO_2–WO_3, CeO_2–WO_3/MCM-22, CeO_2–WO_3-K and CeO_2–WO_3/MCM-22-K catalysts. The above catalysts were characterized by H_2-TPR (Fig. 2a). For CeO_2–WO_3 catalyst, one peak at 559 ℃ attributed to Ce^{4+} and Ce^{4+}-O-Ce^{3+} species on the surface was observed. The CeO_2–WO_3-K catalyst exhibited two reduction peaks at 598 and 630 ℃, which attributable to the reduction of Ce^{4+} and Ce^{4+}-O-Ce^{3+} species on the surface. The CeO_2–WO_3/MCM-22 exhibited four reduction peaks, with the peaks at 551 and 732 ℃ attributable to the reduction of surface oxygen and Ce^{4+} species in the bulk phase, respectively,

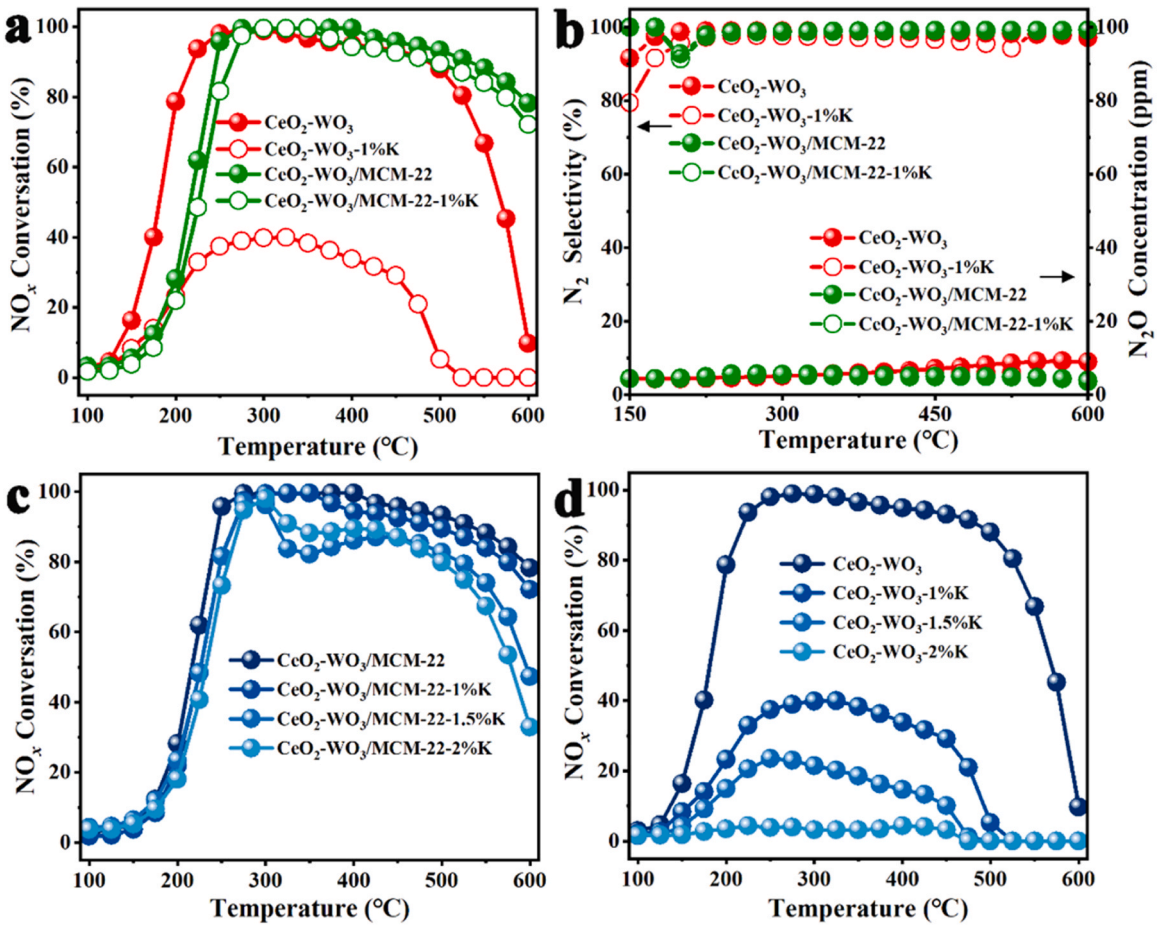

Fig. 1. (a) NO_x conversion, (b) N_2 selectivity and N_2O concentration during the SCR reaction over CeO_2–WO_3, CeO_2–WO_3/MCM-22, CeO_2–WO_3-1%K and CeO_2–WO_3/MCM-22–1%K catalysts; (c) NO_x conversion during the SCR reaction over CeO_2–WO_3/MCM-22-*y*%K and (d) CeO_2–WO_3-*y*%K catalysts. Reaction conditions: [NO] = [NH_3] = 500 ppm, [O_2] = [H_2O] = 5 vol%, N_2 balanced, WHSV = 60,000 mL·$g_{cat.}^{-1}$·h^{-1}.

while the peaks at 814 and 938 ℃ attributable to the reduction of W^{6+} → W^0. The CeO_2–WO_3/MCM-22-K exhibited three reduction peaks, with the peaks at 558 and 736 ℃ attributable to the reduction of surface oxygen and Ce^{4+} species in the bulk phase, while the peak at 938 ℃ attributable to the reduction of W^{6+} → W^0 [26,27]. The reduction temperature of CeO_2–WO_3-K catalyst increased to a higher temperature by 39 ℃ from 559 to 598 ℃, while the reduction temperature of the CeO_2–WO_3/MCM-22-K shifted slightly to high temperature, with a temperature increase of < 10 ℃. In addition, compared with CeO_2–WO_3, the reduction temperature of surface oxygen decreased to a lower temperature, indicating Ce^{4+} was more easily reduced with the MCM-22 and thus improved the NO_x reduction activity. It was well recognized that the acid sites and redox sites are crucial for rendering a SCR catalyst with high-performance, which influence the adsorption/activation of NH_3 and NO_x [28]. These results indicated that the reducibility of the CeO_2–WO_3/MCM-22 catalyst expressed no obvious variation, which corresponded to the activity test results". Thus, the maintained reducing property of the CeO_2–WO_3/MCM-22 catalyst was an important factor that contributed to the excellent K resistance.

Acidity is a crucial parameter for catalytic performance, as NH_3 species were absorbed on acid sites, which was a prerequisite for the NH_3-SCR reaction [29]. Foreign K poisons typically occupied the acid sites of the catalyst, inhibiting the NH_3 adsorption, hindering the *de*NO_x reaction, and significantly reducing the catalytic activity [30]. To investigate the impact of K poisons on catalyst acidity, NH_3-TPD tests were conducted on CeO_2–WO_3, CeO_2–WO_3/MCM-22, CeO_2–WO_3-K and CeO_2–WO_3/MCM-22-K (Fig. 2b). The CeO_2–WO_3/MCM-22 exhibited three desorption peaks corresponding to weak NH_3 adsorption < 300 ℃ and strong NH_3 adsorption > 300 ℃ [31]. The strong acid amount of CeO_2–WO_3/MCM-22-K was reduced, and the overall acid content remained high (Fig. S10). The CeO_2–WO_3 exhibited two desorption peaks corresponding to weak NH_3 adsorption, and the acid amount decreased after K poisoning. In addition, quantitative results further revealed detailed information on the amount of NH_3 desorption (Table S3). The total acid content of the CeO_2–WO_3/MCM-22 was 8.4 mmol·g^{-1}, which was 4.4 times higher than that of CeO_2–WO_3 (1.9 mmol·g^{-1}), indicating that the introduction of MCM-22 increased both acidity and acid sites [32]. This increase was attributable to the presence of L acid sites on the tetrahedral Al site of the molecular sieve and B acid sites in the molecular sieve skeleton. The total acid content of CeO_2–WO_3/MCM-22-K reached 5.5 mmol·g^{-1}, which was ~2.9 times that of fresh CeO_2–WO_3 (1.9 mmol·g^{-1}). These results indicating that CeO_2–WO_3/MCM-22 exhibited high acidity, and the CeO_2–WO_3/MCM-22-K catalyst also exhibited a higher acid content than the CeO_2–WO_3 catalyst.

The oxidation states and concentrations of surface metal elements were analyzed, and XPS tests were conducted on CeO_2–WO_3, CeO_2–WO_3/MCM-22, CeO_2–WO_3-K and CeO_2–WO_3/MCM-22-K. The XPS spectra of Ce, O and W were shown in Fig. 2c, d and Fig. S11, and the corresponding concentration of elements were summarized in Table S3. The catalysts peaks were calibrated to 284.8 eV on the C 1 s peak. The XPS spectra of Ce 3d from various catalysts were observed, and no significant binding energy (BE) shift was observed in Ce between CeO_2–WO_3/MCM-22 and CeO_2–WO_3/MCM-22-K (Fig. 2c). Meanwhile, no apparent change was observed in Ce^{3+}/Ce ratio (25.1% vs. 21.1%). In contrast, the Ce^{3+}/Ce ratio exhibited a noticeable loss (28.3% vs.

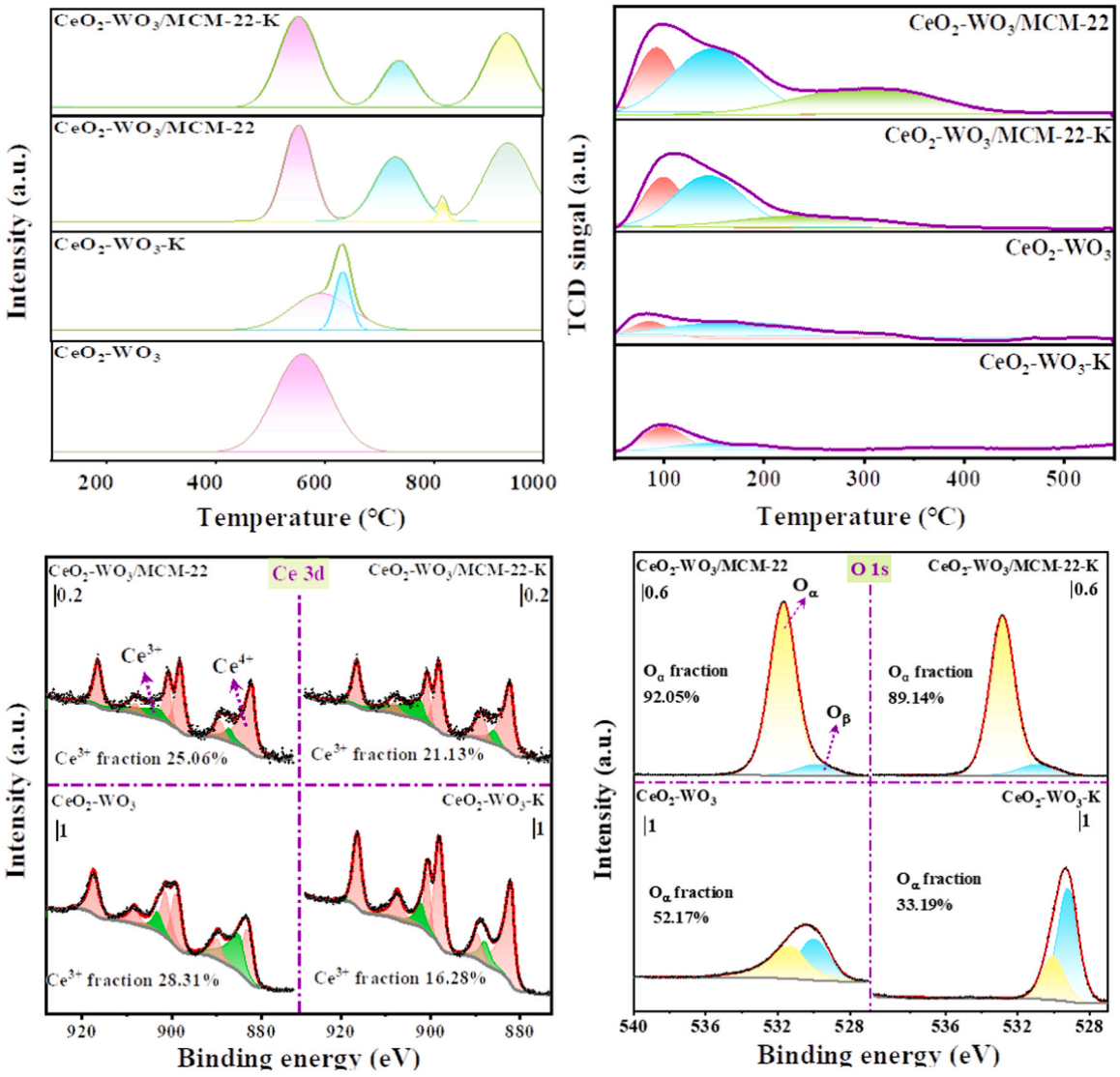

Fig. 2. (a) H_2-TPR and (b) NH_3-TPD profiles for CeO_2–WO_3, CeO_2–WO_3/MCM-22, CeO_2–WO_3-K and CeO_2–WO_3/MCM-22-K; (c) XPS of Ce *3d* and (d) O *1 s* for CeO_2–WO_3, CeO_2–WO_3/MCM-22, CeO_2–WO_3-K and CeO_2–WO_3/MCM-22-K.

16.3%) on CeO_2–WO_3 and CeO_2–WO_3-K. It has been reported that Ce^{3+} can react with O_2 to form O–Ce^{4+} species, which can activate the NH_3 adsorbed on the W═O species of cerium tungstate. According to previously published literature [33], the increased O–Ce^{4+} formation promoted the redox cycle on the CeO_2–WO_3/MCM-22 catalyst". Fig. 2d depicts the XPS spectra of O 1 s from the catalysts, and the fitting peaks of BE at 531.0–533.0 eV and 529.0–531.0 eV were attributable to the chemisorbed oxygen (denoted O_α) and lattice oxygen (denoted O_β), respectively [34,35]. In the quantitative calculation of the O_α/O ratio from various catalysts, a negligible reduction in the O_α/O ratio was observed on CeO_2–WO_3/MCM-22 and CeO_2–WO_3/MCM-22-K (92.1% vs. 89.1%). Compared with CeO_2–WO_3, CeO_2–WO_3/MCM-22 exhibiting higher O_α/O ratio, it can be reasonably speculated that the hydroxyl groups on the molecular sieve MCM-22 adsorbed abundant oxygen However, the O_α/O ratio exhibited a significant decrease (52.2% vs. 33.2%) on CeO_2–WO_3 and CeO_2–WO_3-K. Generally, O_α exhibited higher reactivity than O_β owing to its high reactivity mobility, which was beneficial to the SCR reaction [36,37]. The XPS spectra of W 4 f from the catalysts were observed (Fig. S11). Two distinct peaks in the BE of 32.0–48.0 eV was observed, which were consistent with the W 4 $f_{7/2}$ and W 4 $f_{5/2}$ peaks of pure WO_3, indicating that W element existed in the form of W^{6+} in the catalyst. Meanwhile, the CeO_2–WO_3-K exhibited a WO_3 loss feature peak at 42.0 eV (Fig. S11). According to the above results, compared with CeO_2–WO_3, the ratio of Ce^{3+}, and O_α on CeO_2–WO_3/MCM-22-K exhibited no apparent variation. Combining the experimental results of H_2-TPR and NH_3-TPD, it is inferred that acid sites introduced by MCM-22 tend to preferentially combine with foreign poisons K as sacrificial sites, thus effectively alleviating K-induced deactivation of CeO_2–WO_3.

3.3. Adsorption performance of gas molecules on CeO_2–WO_3/MCM-22-K catalyst

According to the NH_3-TPD results and *de*NO_x reaction performed, the K element was deposited at the acid site on the surface of MCM-22 in the CeO_2–WO_3/MCM-22-K catalyst. Thus, the K element simulated the poisoning process of CeO_2–WO_3/MCM-22 catalysts. Fig. S12 exhibited the model of the optimized CeO_2–WO_3/MCM-22-K catalyst structure. It was observed that K was steadily adsorbed in molecular sieve MCM-22, which effectively protected the active CeO_2–WO_3 component from deactivation by K poisoning. Further confirming our previous speculation, the introduced acid sites of the molecular sieve MCM-22 were used as sacrificial sites to trap foreign K poison, thus, the loss of activity was restored. To elucidate the adsorption performance and analyze

interatomic interactions on CeO_2–WO_3/MCM-22-K, the adsorption energy (E_{ads}) and projected density of states (PDOS) of NO, NO_2, NH_3 and O_2 gas molecules on CeO_2–WO_3/MCM-22-K surface were studied (Fig. 3). The calculated E_{ads} of all gas molecules on CeO_2–WO_3/MCM-22-K surface were < 0, indicating that the reactant gas molecules were easily adsorbed on CeO_2–WO_3/MCM-22-K surface, which was beneficial to NH_3-SCR reaction. The overlap of W 5d and N 2p orbitals in NO in a wide range was attributable to interorbital hybridization, indicating a strong interaction between NO and the catalyst, thus, a strong adsorption of NO was observed on the catalyst. Similarly, strong interactions between NO, NO_2, NH_3 and O_2 gas molecules and CeO_2–WO_3/MCM-22-K catalyst were observed, indicating that the reactant gas molecules were strongly adsorbed on the CeO_2–WO_3/MCM-22-K catalyst surface. These results corresponded to the experimental results, confirming that the acid sites of MCM-22 molecular sieve acted as sacrificial sites and prevented the active component against K poisoning.

3.4. Reaction mechanism analysis

To elucidate reactive species and reaction mechanism, in situ diffuse reflectance infrared Fourier transform spectroscopy (DRIFTs) characterization was conducted on the catalysts. Initially, the catalysts were pretreated in N_2 air flow (45 mL·min^{-1}) at 400 ℃ for 1 h to remove surface moisture and impurities. The catalysts were treated in NH_3 air flow (5 mL·min^{-1}) for 1 h, and the in situ DRIFTs of NH_3 adsorption over CeO_2–WO_3 and CeO_2–WO_3/MCM-22 were observed (Fig. S14a,b). Several signal peaks ascribed to asymmetric bending vibration of ionic NH_4^+ (1471 cm^{-1}), asymmetric and symmetric bending vibrations of coordinated NH_3 (1600 and 1288 cm^{-1}) were detected on CeO_2–WO_3/MCM-22 after the NH_3 adsorption [38]. Meanwhile, several signals belonging to symmetric and asymmetric bending vibrations of ionic NH_4^+ (1666 and 1421 cm^{-1}), asymmetric and symmetric bending vibrations of coordinated NH_3 (1591 and 1180 cm^{-1}) were detected on CeO_2–WO_3 after the adsorption of NH_3 [39–41]. These results indicated

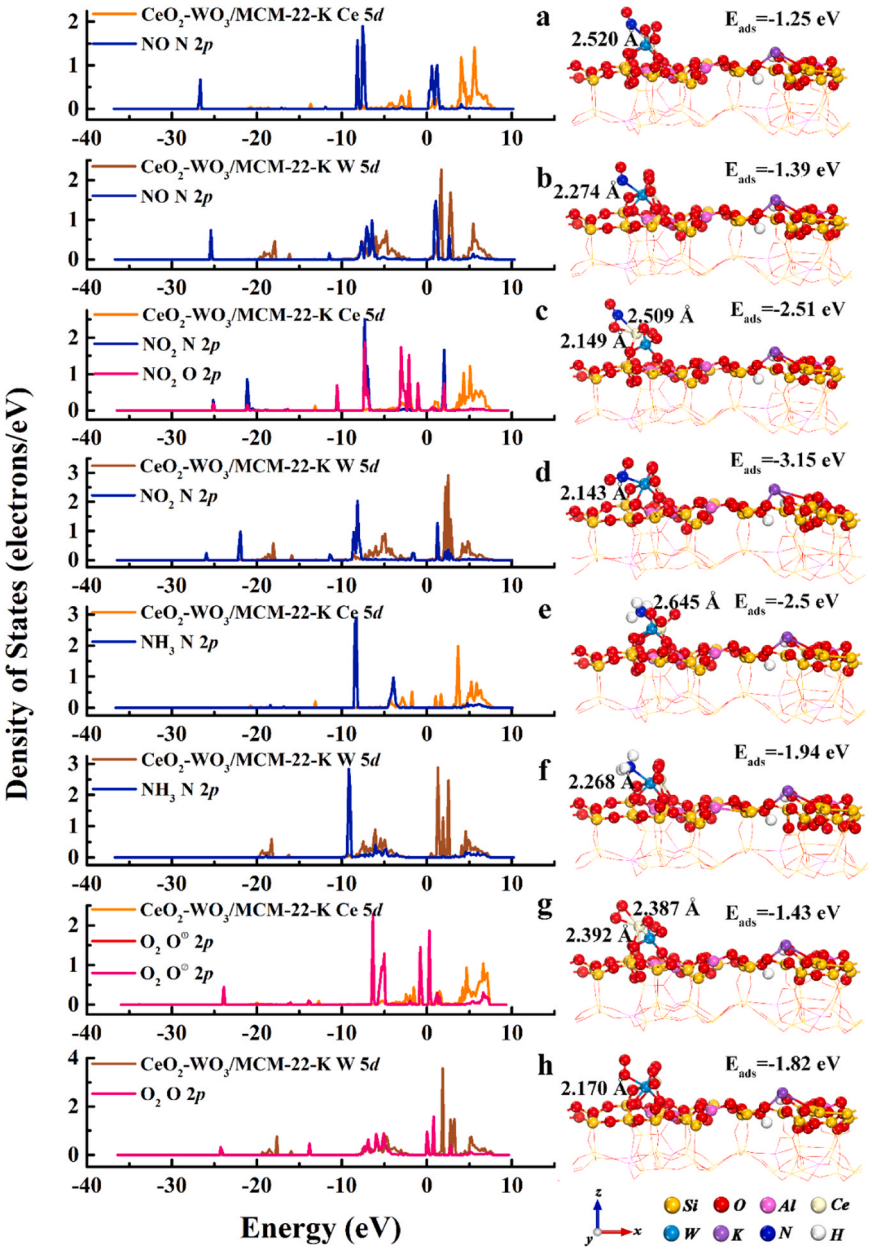

Fig. 3. (a–h) Adsorption configurations, adsorption energy (E_{ads}) and Project density of states (PDOS) of NO, NO_2, NH_3 and O_2 gas molecules on the CeO_2–WO_3/MCM-22-K catalyst surface, respectively.

that both CeO_2–WO_3 and CeO_2–WO_3/MCM-22 contained abundant acid sites, which were used for NH_3 adsorption. Fig. S14c,d shows the in situ DRIFTs results of NO+O_2 reaction with pre-adsorbed NH_3 over CeO_2–WO_3 and CeO_2–WO_3/MCM-22 at 200 ℃. For CeO_2–WO_3/MCM-22, the peaks assigned to B (1471 cm^{-1}) and L (1600 and 1288 cm^{-1}) acid sites were detected. After passing NO+O_2, the B acid sites and L acid sites diminished within 40 min. Simultaneously, the bidentate nitrate species exhibited a signal peak (1579 cm^{-1}). Compared with CeO_2–WO_3, the peaks attributable to B (1666 and 1421 cm^{-1}) and L (1591 and 1180 cm^{-1}) acid sites were observed. After passing NO+O_2, the peak of ammonia species adsorbed on B acid sites and L acid sites disappeared within 30 min. Simultaneously, the adsorbed NO_2 species exhibited the signal peak (1604 cm^{-1}), indicating that the "Fast–SCR" reaction occurred on CeO_2–WO_3. The in situ DRIFTs results of NH_3 reaction with pre-adsorbed NO+O_2 over CeO_2–WO_3 and CeO_2–WO_3/MCM-22 (Fig. S13). The catalyst was treated in a NO+O_2

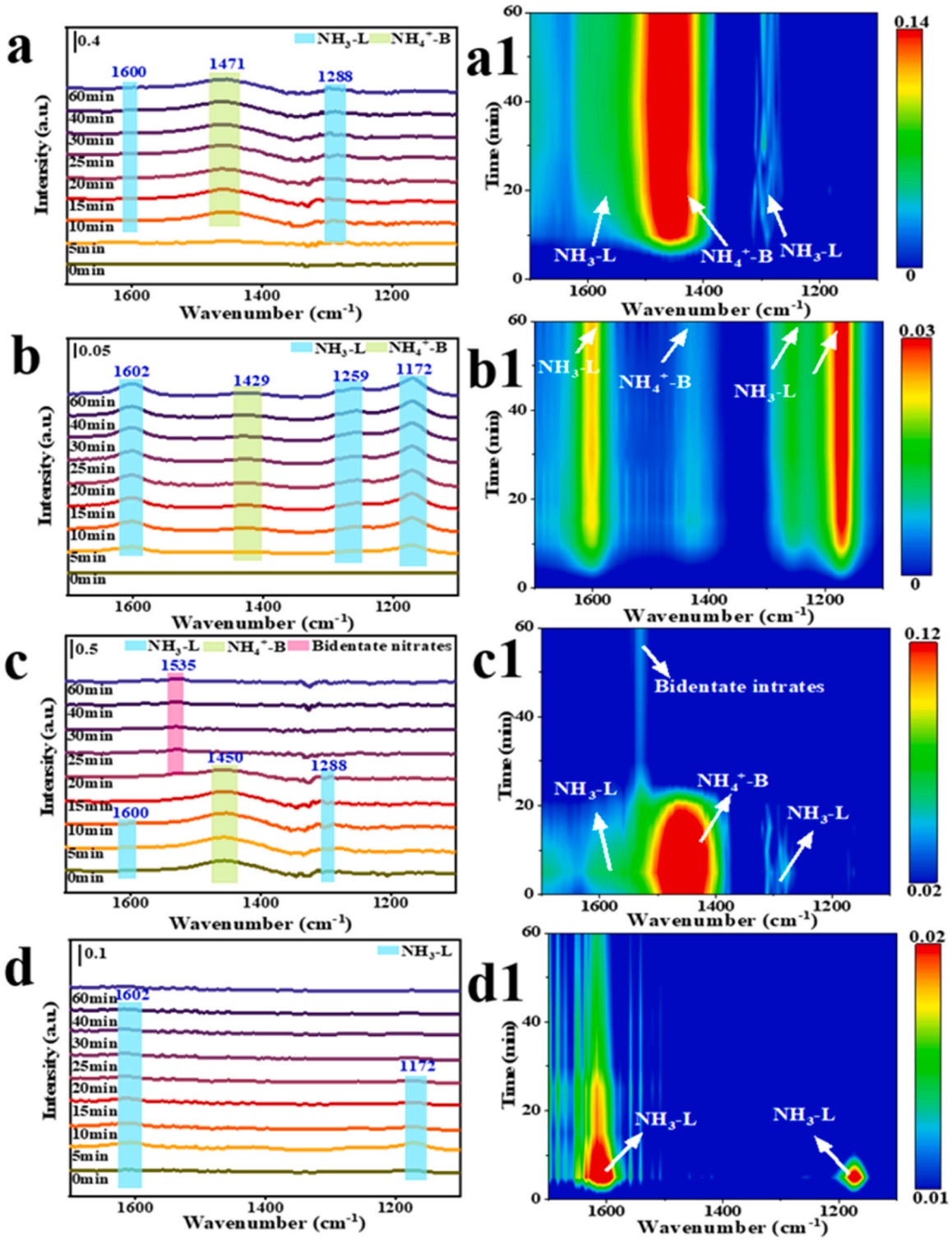

Fig. 4. The transient NH_3 adsorption DRIFTs profiles and the corresponding mapping results over (a, a_1) CeO_2–WO_3/MCM-22-K and (b, b_1) CeO_2–WO_3-K; *In situ* DRIFTs of the transient reactions between NO+O_2 and pre–adsorbed NH_3 over (c, c_1) CeO_2–WO_3/MCM-22-K and (d, d_1) CeO_2–WO_3-K measured at 200 ℃.

atmosphere for 1 h, purged with pure N_2 for 30 min to remove the physically absorbed NO_x species, and finally exposed to an NH_3 atmosphere for 1 h. The peaks attributable to bidentate nitrate (1579 cm^{-1}) were exhibited in CeO_2–WO_3/MCM-22. After exposure to NH_3, peaks attributable to B acid sites and L acid sites were observed and the peaks assigned to the bidentate were covered. It was observed that no significant difference occurred when reaction gases were fed into the catalyst in reverse order, indicating a weak or no reaction between nitrate species and NH_3 species. NH_3 adsorbed on the catalyst reacted directly with NO + O_2, and the catalytic reaction followed E–R mechanism. The CeO_2–WO_3, the nitrate (1232 cm^{-1}) and adsorbed NO_2 species (1604 cm^{-1}) were observed on the catalyst by purging NO + O_2 [42]. After exposure to NH_3, the peak attributable to adsorbed NO_2 species significantly decreased within 10 min, and then peaks attributable to B acid sites (1666 and 1421 cm^{-1}) and L acid sites (1591 and 1180 cm^{-1}) were exhibited. It can be inferred that CeO_2–WO_3 followed L–H mechanism.

The introduction of K reduced the acidity of CeO_2–WO_3 and CeO_2–WO_3/MCM-22. *In situ* DRIFTs analysis was conducted to evaluate the effect of K on the adsorption behavior of substances on the catalysts, and the CeO_2–WO_3-K and CeO_2–WO_3/MCM-22-K were characterized (Fig. 4). After K poisoning, the position of CeO_2–WO_3/MCM-22-K signal peaks exhibited no significant variation, indicating that there were still abundant acid sites on the catalyst for NH_3 adsorption (Fig. 4a). It was plausible that the acid sites of MCM-22 tended to combine with the foreign alkali poisons K as sacrificial sites, thus the active Ce–W component was retained. However, the CeO_2–WO_3-K, the faint peaks belonging to L (1602, 1259 and 1172 cm^{-1}) and B (1429 cm^{-1}) acid sites were observed after NH_3 adsorption [43], indicating that K significantly reduced the acid sites especially the B acid sites on CeO_2–WO_3-K. In a previous study [18], NH_3 adsorption occurred at the B acid sites formed by the W═O bond on cerium tungstate, indicating that K inhibited the adsorption of NH_3 by occupying the B acid site of CeO_2–WO_3, thus hindering the NH_3–SCR reaction and leading to the conspicuous deactivation of the catalyst. The in situ DRIFTs results of NO+O_2 reaction with pre-adsorbed NH_3 over CeO_2–WO_3-K and CeO_2–WO_3/MCM-22-K at 200 ℃ (Fig. 4c, d). The peaks attributable to B (1471 cm^{-1}) and L (1288 cm^{-1}) acid sites were detected on the CeO_2–WO_3/MCM-22-K catalyst. After passing NO+O_2, both B and L acid sites vanished within 30 min. Simultaneously, the peak attributable to bidentate nitrate (1535 cm^{-1}) was observed (Fig. 4c). Conversely, the weak peaks attributable to L acid sites (1602 and 1172 cm^{-1}) were observed on CeO_2–WO_3-K (Fig. 4d). After the introduction of NO+O_2, the L acid sites was reduced slightly, indicating that K severely inhibited NH_3-SCR reaction on CeO_2–WO_3.

The in situ DRIFTs results of NH_3 reaction with pre-adsorbed NO+O_2 over CeO_2–WO_3-K and CeO_2–WO_3/MCM-22-K were observed (Fig. S15). The peak attributable to bidentate nitrate (1535 cm^{-1}) appeared on CeO_2–WO_3/MCM-22-K. After exposure to NH_3, the peaks attributable to B acid sites (1473 cm^{-1}) and L acid sites (1600 and 1288 cm^{-1}) were observed within 10 min and the peak attributable to bidentate nitrate were covered (Fig. S15a). It was observed that no significant difference occurred on CeO_2–WO_3/MCM-22 after K was introduced. The slight signal peaks of L acid sites (1602, 1259 and 1172 cm^{-1}) were detected on CeO_2–WO_3-K after NH_3 adsorption (Fig. S15b). In previous study [18], gaseous NH_3 did not react directly with NO on CeO_2–WO_3, indicating that the main reason for the deactivation of CeO_2–WO_3 was that K occupied the B acid sites of W═O species on cerium tungstate. Thus, inhibiting the adsorption of NH_3 species, and seriously hindering the E–R reaction path. However, for CeO_2–WO_3/MCM-22-K, the K preferentially combined with the acid sites of the MCM-22 molecular sieve, thereby, releasing the occupied B acid site on cerium tungstate and restoring the E–R reaction path. Fig. 5 illustrates the proposed reaction pathways of CeO_2–WO_3-K and CeO_2–WO_3/MCM-22-K. The deactivation effect of K on the CeO_2–WO_3 catalyst primarily resulted in a decrease of B acid sites on cerium tungstate, inhibiting NH_3 adsorption and

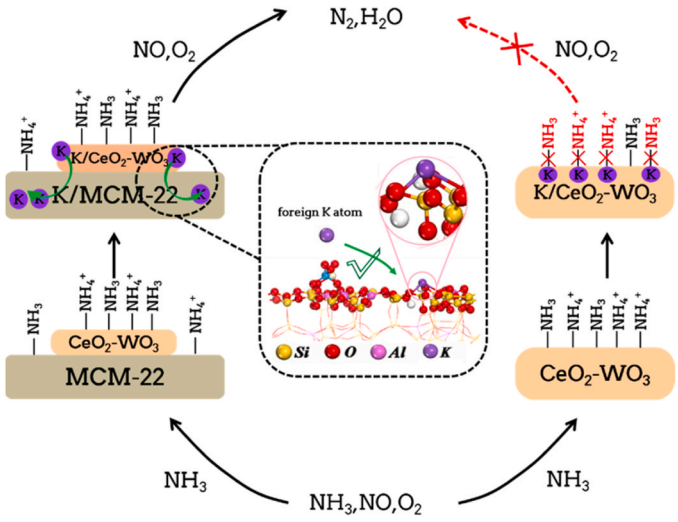

Fig. 5. Schematic illustration of the anti–K poisoning mechanism on CeO_2–WO_3 and CeO_2–WO_3/MCM-22 catalysts.

hindering the E–R pathway. In contrast, the acid sites of the MCM-22 molecular sieve on the CeO_2–WO_3/MCM-22-K preferentially combined with K as sacrificial sites, protecting the active CeO_2–WO_3 component and restoring the E–R reaction path. Therefore, CeO_2–WO_3/MCM-22 catalyst exhibited conspicuous K tolerance. In this study, the finding provides a theoretical foundation for the development of an environmentally friendly NH_3-SCR catalyst with exceptional K resistance.

4. Conclusions

In summary, compared with CeO_2–WO_3 catalyst, CeO_2–WO_3/MCM-22 catalyst exhibited minimal activity loss after 1 wt% K poisoning and maintained good activity after 2 wt% K poisoning. The incorporation of layered molecular sieve MCM-22 resulted in an increased number of strong acid sites in the CeO_2–WO_3/MCM-22 catalyst, which facilitated high-temperature NH_3-SCR reaction. In the case of CeO_2–WO_3 catalyst, K occupied the B acid sites formed by W═O species on the cerium tungstate and decreased the redox performance of the CeO_2–WO_3 catalyst. Thus, inhibiting the adsorption of NH_3 species and limiting the redox cycle (NH_3 activation), which combination led to the slow reaction rate and severe deactivation of the CeO_2–WO_3 catalyst. However, the CeO_2–WO_3/MCM-22 catalyst, due to the acid-base coordination theory, the acid sites of zeolite MCM-22 preferentially combined with foreign K poisons, which acted as sacrificial sites to protect the occupied B acid sites on the cerium tungstate and restore the acid site cycle for NH_3 adsorption. Moreover, the reduction performance and the ratio of Ce^{3+} and O_α were well maintained in the CeO_2–WO_3/MCM-22 catalyst after K poisoning. Generally, the CeO_2–WO_3/MCM-22 catalyst exhibited excellent denitrification activity and prominent K resistance.

CRediT authorship contribution statement

Liu Wenming: Resources, Methodology. **Li Yonglong:** Methodology, Investigation. **Li Guobo:** Writing – review & editing, Supervision, Project administration, Funding acquisition. **Chen Lei:** Writing – review & editing, Writing – original draft, Methodology, Formal analysis, Data curation. **Zou Yu:** Methodology, Investigation. **Peng Honggen:** Writing – review & editing, Supervision, Project administration, Funding acquisition. **Li Zhenguo:** Methodology, Investigation. **Zhang Shule:** Methodology, Investigation. **Zhang Hongxiang:** Methodology, Investigation. **Lu Shengyong:** Resources, Methodology.

Declaration of Competing Interest

The authors declare that they have no known competing financial interests or personal relationships that could have appeared to influence the work reported in this paper.

Data availability

Data will be made available or request. No data was used for the research described in the article.

Acknowledgements

This work was supported by the National Natural Science Foundation of China (22276086, 21976078 and 22306086), the Natural Science Foundation of Jiangxi Province (20202ACB213001 and 20232BAB213028), the National Engineering Laboratory for Mobile Source Emission Control Technology (NELMS2019A12), the State Key Laboratory of Clean Energy Utilization (ZJUCEU2022015), and the Natural Science Foundation of Chongqing (CSTB2023NSCQ-MSX0950), all of which are greatly acknowledged by the authors.

Appendix A. Supporting information

Supplementary data associated with this article can be found in the online version at doi:10.1016/j.apcatb.2024.123788.

References

[1] Y. Yu, W. Tan, D. An, X. Wang, A. Liu, W. Zou, C. Tang, C. Ge, Q. Tong, J. Sun, Insight into the SO_2 resistance mechanism on γ-Fe_2O_3 catalyst in NH_3-SCR reaction: a collaborated experimental and DFT study, Appl. Catal. B Environ. 281 (2021) 119544.
[2] Y. Li, H. Chen, L. Chen, Y. Zhang, Y. Mi, M. Liao, W. Liu, D. Wu, Z. Li, Ternary $MnCoVO_x$ catalysts with remarkable deNO_x performance: dual acid-redox sites control strategy. Appl. Catal. B Environ. 318 (2022) 121779.
[3] M. Guo, B. Lis, M. Ford, I. Wachs, Effect of redox promoters (CeO_x and CuO_x) and surface sulfates on the selective catalytic reduction (SCR) of NO with NH_3 by supported V_2O_5-WO_3/TiO_2 catalysts, Appl. Catal. B Environ. 306 (2022) 121108.
[4] G. Li, Y. Li, D. Han, W. Liu, M. Liao, L. Chen, D. Wu, Z. Li, L. Wei, S. Lu, H. Peng, Unraveling alkali-tolerance role of zeolite coupling $CeWO_x$ catalyst for NO_x reduction, Appl. Catal. B Environ. 334 (2023) 122872.
[5] J. Deng, S. Cai, M. Gao, J. Hasegawa, H. Yao, Y. Shen, Z. Si, J. Song, D. Zhang, Crystal-in-Amorphous vanadate catalysts for universal Poison-Resistant elimination of nitric oxide, ACS Catal. 13 (2023) 12363–12373.
[6] Z. Si, Y. Shen, J. He, T. Yan, J. Zhang, J. Deng, D. Zhang, SO_2-induced alkali resistance of $FeVO_4$/TiO_2 catalysts for NO_x reduction, Environ. Sci. Technol. 56 (2022) 605–613.
[7] Z. Jia, Y. Shen, T. Yan, H. Li, J. Deng, J. Fang, D. Zhang, Efficient NO_x abatement over alkali-resistant catalysts via constructing durable dimeric VO_x species, Environ. Sci. Technol. 56 (2022) 2647–2655.
[8] Y. Dong, P. Wang, X. Liu, J. Deng, A. Chen, L. Han, D. Zhang, Alkali-resistant NO_x reduction over $FeVO_4$/TiO_2 catalysts via regulating the electron transfer between Fe and V, Chin. Chem. Lett. (2023) 108635.
[9] C. Feng, P. Wang, X. Liu, F. Wang, T. Yan, J. Zhang, G. Zhou, D. Zhang, Alkali-resistant catalytic reduction of NO_x via naturally coupling active and poisoning sites, Environ. Sci. Technol. 55 (16) (2021) 11255–11264.
[10] P. Zhang, P. Wang, A. Chen, L. Han, T. Yan, J. Zhang, D. Zhang, Alkali–resistant catalytic reduction of NO_x by using Ce–O–B alkali–capture sites, Environ. Sci. Technol. 55 (2021) 11970–11978.
[11] J. Ji, Y. Tang, L. Han, P. Ran, W. Song, Y. Cai, W. Tan, J. Sun, C. Tang, L. Dong, Cerium manganese oxides coupled with ZSM–5: a novel SCR catalyst with superior K resistance, Chem. Eng. J. 445 (2022) 136530.
[12] S. Chen, R. Xie, Z. Liu, N. Yan, L. Ma, Efficient NO_x reduction against alkali poisoning over a self–protection armor by fabricating surface $Ce_2(SO_4)_3$ species: comparison to commercial vanadia catalysts, Environ. Sci. Technol. 57 (2023) 2949–2957.
[13] J. Zhou, P. Wang, A. Chen, W. Qu, Y. Zhao, D. Zhang, NO_x reduction over smart catalysts with self-created targeted anti-poisoning sites, Environ. Sci. Technol. 56 (2022) 6668–6677.
[14] J. Liu, X. Shi, Z. Lv, Y. Yu, H. He, Ceria-tungsten-tin oxide catalysts with superior regeneration capacity after sulfur poisoning for NH_3-SCR process. Catal. Sci. Technol. 12 (2022) 2471–2481.
[15] S. Li, H. Yu, T. Lan, L. Shi, D. Cheng, L. Han, D. Zhang, NOx reduction against alkali poisoning over $Ce(SO_4)_2$-V_2O_5/TiO_2 catalysts by constructing the Ce^{4+}–SO_4^{2-} pair sites, Chin. Chem. Lett. (2023) 108240.
[16] W. Shan, F. Liu, H. He, X. Shi, C. Zhang, Novel cerium-tungsten mixed oxide catalyst for the selective catalytic reduction of NO_x with NH_3, Chem. Commun. 47 (2011) 8046–8048.
[17] Y. Peng, J. Li, L. Chen, J. Chen, J. Han, H. Zhang, W. Han, Alkali metal poisoning of a CeO_2–WO_3 catalyst used in the selective catalytic reduction of NO_x with NH_3: an experimental and theoretical study, Environ. Sci. Technol. 46 (2012) 2864–2869.
[18] Y. Peng, K. Li, J. Li, Identification of the active sites on CeO_2–WO_3 catalysts for SCR of NO_x with NH_3: an in situ IR and Raman spectroscopy study, Appl. Catal. B Environ. 140–41 (2013) 483–492.
[19] A. Schwanke, S. Pergher, Lamellar MWW–type molecular sieves: toward elegant nanoporous materials, Appl. Sci. 8 (2018) 1636.
[20] M. Nawab, S. Barot, R. Bandyopadhyay, Solvent–free selective oxidation of toluene over metal–doped MCM–22, New. J. Chem. 43 (2019) 4406–4412.
[21] J. González, J. Wang, L. Chen, M. Manríquez, J. Dominguez, Structural defects, lewis acidity, and catalysis properties of mesostructured WO_3/SBA-15 nanocatalysts, J. Phys. Chem. C 121 (2017) 23988–23999.
[22] A.–S. Mamede, E. Payen, P. Grange, G. Pomcelet, M. Alifanti, V.I. Pârvulescu, Characterization of WO_x/CeO_2 catalysts and their reactivity in the isomerization of hexane. J. Catal. 223 (2004) 1–12.
[23] J. Liu, H. Cheng, H. Zheng, L. Zhang, B. Liu, W. Soong, J. Liu, W. Zhu, H. Li, Z. Zhao, Insight into the potassium poisoning effect for selective catalytic reduction of NO_x with NH_3 over Fe/Beta, ACS Catal. 11 (2021) 14727–14739.
[24] X. Du, X. Gao, K. Qiu, Z. Luo, K. Cen, The reaction of poisonous alkali oxides with vanadia SCR catalyst and the afterward influence: a DFT and experimental study, J. Phys. Chem. C 119 (2015) 1905–1912.
[25] T. Andana, K. Rappé, N. Nelson, F. Gao, Y. Wang, Selective catalytic reduction of NO_x with NH_3 over Ce–Mn oxide and Cu–SSZ–13 composite catalysts – low temperature enhancement, Appl. Catal. B Environ. 316 (2022) 121522.
[26] B. Liu, J. Liu, L. Xin, T. Zhang, Y. Xu, F. Jiang, X. Liu, Unraveling reactivity descriptors and structure sensitivity in low–temperature NH_3–SCR reaction over $CeTiO_x$ catalysts: a combined computational and experimental study, ACS Catal. 11 (2021) 7613–7636.
[27] C. Liu, Y. Bi, H. Wang, Z. Zhang, J. Wang, M. Gou, Q. Liu, Promotional effects on NH_3–SCR performance of CeO_2–SnO_2 catalysts doped by TiO_2: a mechanism study, Catal. Surv. Asia 25 (2021) 48–57.
[28] R. Yu, Z. Zhao, C. Shi, W. Zhang, Insight into the synergic effect of Fe–SSZ–13 molecular sieve and $FeMnTiZrO_x$ catalyst with enhanced reactivity in NH_3–SCR of NO_x, J. Phys. Chem. C 123 (2019) 2216–2227.
[29] Y. Li, H. Chen, L. Chen, Y. Zhang, Y. Mi, M. Liao, W. Liu, D. Wu, Z. Li, H. Peng, Ternary $MnCoVO_x$ catalysts with remarkable *de*NO_x performance: dual acid–redox sites control strategy, Appl. Catal. B Environ. 318 (2022) 121779.
[30] L. Yan, Y. Ji, P. Wang, C. Feng, L. Han, H. Li, T. Yan, L. Shi, D. Zhang, Alkali and phosphorus resistant molecular sieve–like catalysts for NO_x reduction by NH_3, Environ. Sci. Technol. 54 (2020) 9132–9141.
[31] R. Yu, Z. Zhao, C. Shi, W. Zhang, Insight into the synergic effect of Fe–SSZ–13 molecular sieve and $FeMnTiZrO_x$ catalyst with enhanced reactivity in NH_3–SCR of NO_x, J. Phys. Chem. C 123 (2019) 2216–2227.
[32] X. Wang, Y. Ma, Q. Wu, Y. Wen, F. Xiao, Molecular sieve nanosheets for catalysis, Chem. Soc. Rev. 51 (2022) 2431–2443.
[33] W. Shan, F. Liu, H. He, X. Shi, C. Zhang, Novel cerium-tungsten mixed oxide catalyst for the selective catalytic reduction of NO_x with NH_3, Chem. Commun. 47 (2011) 8046–8048.
[34] W. Tan, A. Liu, S. Xie, Y. Yan, T. Shaw, Y. Pu, K. Gou, L. Li, S. Yu, F. Gao, F. Liu, L. Dong, Ce–Si mixed oxide: a high sulfur resistant catalyst in the NH_3–SCR reaction through the mechanism–enhanced process, Environ. Sci. Technol. 55 (2021) 4017–4026.
[35] W. Liu, Z. Gao, X. Zhao, J. Gao, R. Yang, L. Yu, Promotion effect of chromium on the activity and SO_2 resistance of CeO_2–TiO_2 catalysts for the NH_3–SCR reaction, Ind. Eng. Chem. Res. 60 (2021) 11676–11688.
[36] Z. Lian, W. Shan, Y. Zhang, M. Wang, H. He, Morphology–dependent catalytic performance of NbO_x/CeO_2 catalysts for selective catalytic reduction of NO_x with NH_3, Ind. Eng. Chem. Res. 57 (2018) 12736–12741.
[37] F. Liu, H. He, Y. Ding, C. Zhang, Effect of manganese substitution on the structure and activity of iron titanate catalyst for the selective catalytic reduction of NO with NH_3, Appl. Catal. B Environ. 93 (2009) 194–204.
[38] B. Wang, M. Wang, L. Han, Y. Hou, W. Bao, C. Zhang, G. Feng, L. Chang, Z. Huang, J. Wang, Improved activity and SO_2 resistance by Sm-modulated redox of $MnCeSmTiO_x$ mesoporous amorphous oxides for low-temperature NH_3-SCR of NO, ACS Catal. 10 (2020) 9034–9045.
[39] Z. Fan, J. Shi, C. Gao, G. Gao, B. Wang, Y. Wang, C. He, C. Niu, Gd-modified MnO_x for the selective catalytic reduction of NO by NH_3: the promoting effect of Gd on the catalytic performance and sulfur resistance, Chem. Eng. J. 348 (2018) 820–830.
[40] Z. Liu, P. Millington, J. Bailie, R. Rajaram, J. Anderson, A comparative study of the role of the support on the behaviour of iron based ammonia SCR catalysts, Microporous Mesoporous Mater. 104 (2007) 159–170.
[41] G. Busca, M.A. Larrubia, L. Arrighi, G. Ramis, Catalytic abatement of NO_x: chemical and mechanistic aspects, Catal. Today 107–108 (2005) 139–148.
[42] Z. Shen, X. Liu, S. Impeng, C. Zhang, T. Yan, P. Wang, D. Zhang, Alkali and heavy metal copoisoning resistant catalytic reduction of NO_x via liberating Lewis acid sites, Environ. Sci. Technol. 56 (2022) 5141–5149.
[43] S. Zhan, M. Qiu, S. Yang, D. Zhu, H. Yu, Y. Li, Facile preparation of MnO_2 doped Fe_2O_3 hollow nanofibers for low temperature SCR of NO with NH_3, J. Mater. Chem. A 2 (2014) 20486–20493.